Supporting Information

NiX Layered Double Hydroxide Nanowire Arrays (X=Co, Fe, and Mn) Coated with Nanometer-Thick Films of NiOOH and then NiO as Electrodes for Supercapacitors

*Thangavel Kavinkumar, Selvaraj Seenivasan and Do-Heyoung Kim**

School of Chemical Engineering, Chonnam National University, 77 Yongbong-ro, Gwangju 61186, Republic of Korea.

*Corresponding author's email: kdhh@chonnam.ac.kr

Tel. (office): +82-62-530-1894

Materials

Cobalt(II) chloride hexahydrate (purity ≥ 98.0%), nickel(II) chloride hexahydrate (purity ≥ 98.0%), iron(III) chloride hexahydrate (purity 97.0%), manganese(II) chloride hexahydrate (purity 98.0%), urea (purity ≥98.0%), AC powder (100 mesh), phosphoric acid (purity ≥ 99.5%), nickel sulfate hexahydrate (purity ≥ 98.0%) and potassium persulfate (purity ≥ 99.0%) were obtained from Sigma-Aldrich. Ammonia solution (25%) was obtained from Merck and absolute ethanol from DAEJUNG (South Korea). Nickel foam (1.6 mm thickness) was purchased from MTI Korea (purity > 99.99%). All chemicals are used as received without further purification.

Material Characterization

XRD pattern was collected using an X-ray diffractometer (PANalytical) with Cu Kα radiation. Morphologies and microstructures were optimized with a FE-SEM (JEOL JSM-7500F) and a TEM, FEI, Tecnai G2 F20 TEM). The oxidation state of the products was analyzed using XPS

system (ESCALAB-MKII (VG Scientific Co.). BET (ASAP 2010, Micromeritics) was tested to determine the specific surface area of the fabricated heteronanostructure electrodes.

Electrochemical measurements

The supercapacitive properties of the prepared heteronanostructure electrodes were executed in 2M KOH aqueous solution using a three-electrode configuration. The constructed binder-free electroactive materials on the NF, Pt foil and SCE was used as working electrode, counter electrode and reference electrode on a WonATech WBCS30000 electrochemical workstation, respectively. The mass of NF before and after the reactions was weighed by Ohaus-Adventurer analytical balance with high resolution. The mass loading of the NiX-LDH (X=Co, Fe and Mn)/NiOOH@ALD-NiO materials onto NF is 3.5 mg (1×1 cm^2). The mass loading of a typical AC (1×1 cm^2) is about 4.2 mg onto NF substrate. The EIS measurement was performed using a Parstat 3000 workstation (0.01 Hz to 100 kHz with a 10 mV amplitude) in the same electrolyte. For the two-electrode cells of ASC, the hierarchical NiCo-LDH/NiOOH@ALD-NiO heteronanostructure employed as the positive electrode and AC as the negative electrode with 2M KOH/PVA gel as the electrolyte.

The specific capacitance and specific capacity of the electrodes is calculated from the GCD curves with the help of following formula,

$$Cs = \frac{I\Delta t}{m\Delta V} \qquad \text{(S1)}$$

$$Cm = \frac{I\Delta t}{m} \qquad \text{(S2)}$$

where, C_s (F g^{-1}) is the specific capacitance, C_m (C g^{-1}) refer to the specific capacity, I (A) is the discharge current, Δt (sec) is the discharge time, ΔV (V) is the potential range, and m (mg) is the mass of the active materials.

For the constructed energy storage device, the mass ratio between the two electrodes is calculated according to the following formula,

$$\frac{m^+}{m^-} = \frac{C^- X \Delta V^-}{C^+ X \Delta V^+} \qquad \text{(S3)}$$

where C^-, C^+ are the specific capacitance and m^- and m^+ are the mass of the negative and positive electrodes, ΔV^- and ΔV^+ denotes the voltage window of the two electrodes, respectively. The energy density (E) and power density (P) of ASC device is calculated according to the following formula

$$E = \frac{C\Delta V^2}{7.2} \qquad (Wh\ kg^{-1}) \quad \text{(S4)}$$

and

$$P = \frac{3600\ E}{\Delta t} \qquad (W\ kg^{-1}) \quad \text{(S5)}$$

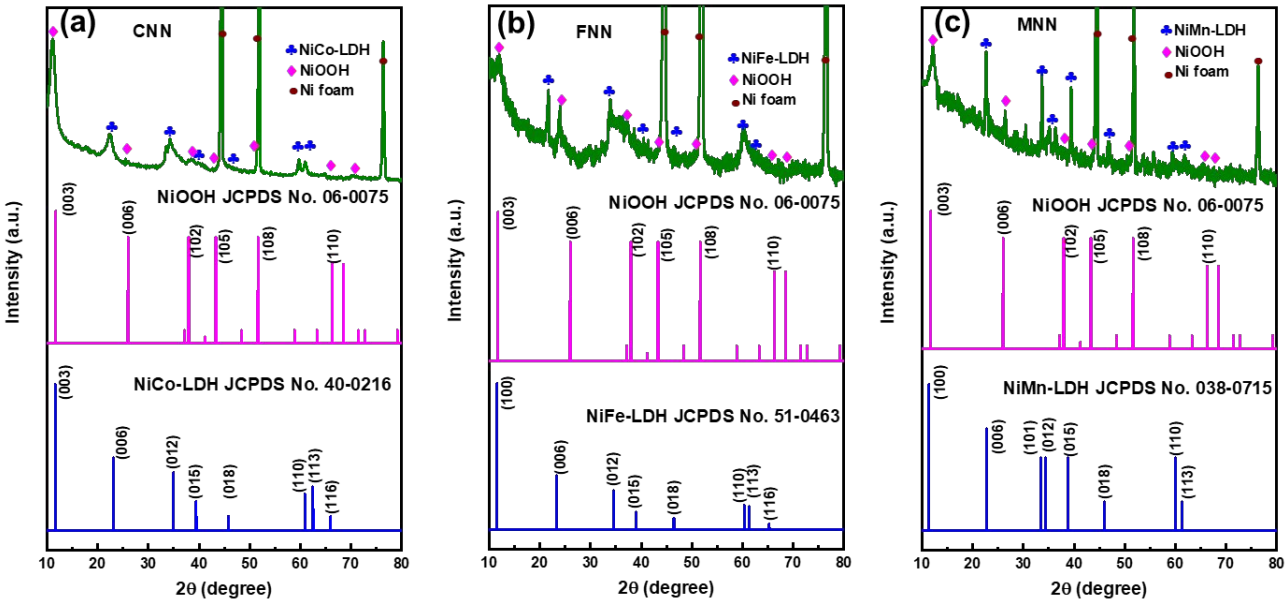

Figure S1. XRD patterns of a) CNN, b) FNN and c) MNN.

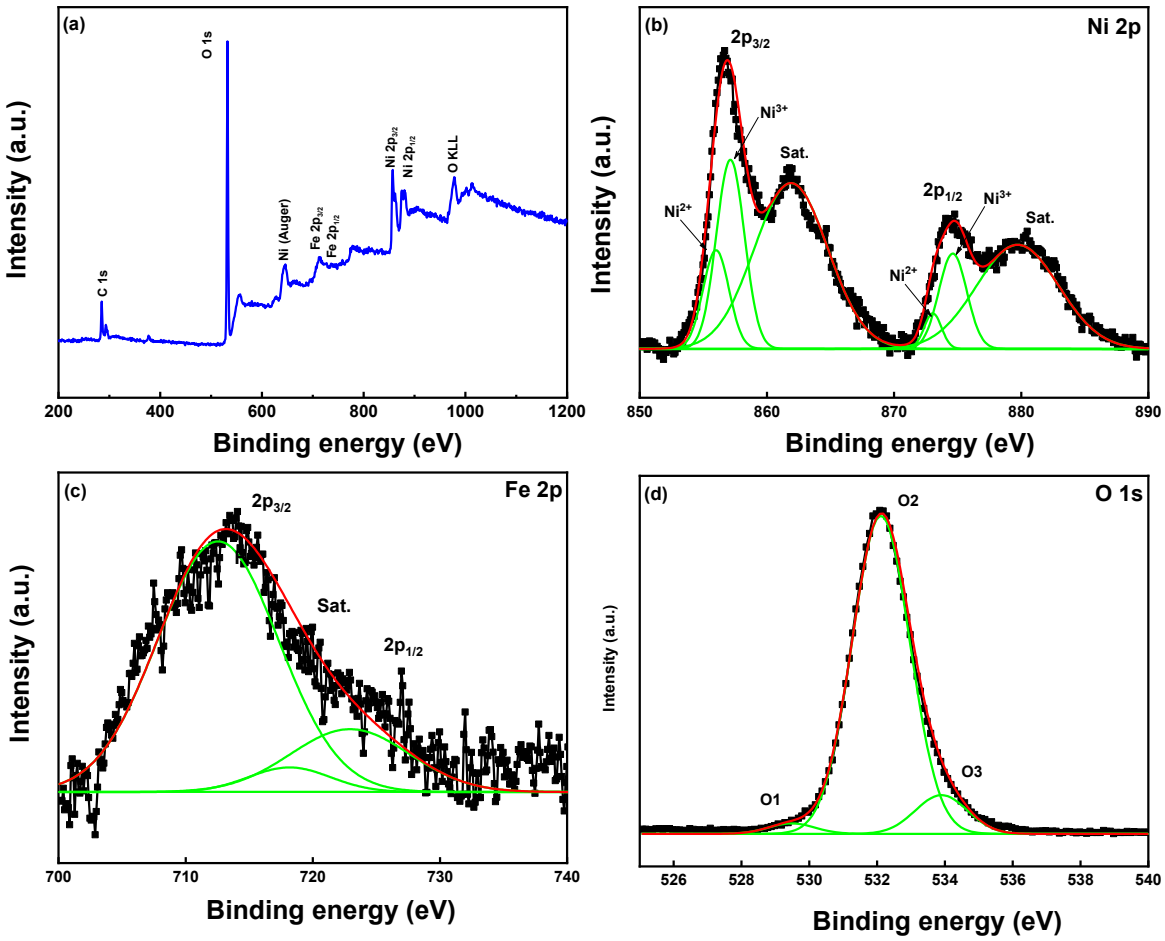

Figure S2. XPS a) survey and high-resolution spectra of b) Ni 2p, c) Fe 2p, and d) O 1s of the FNN heteronanostructure.

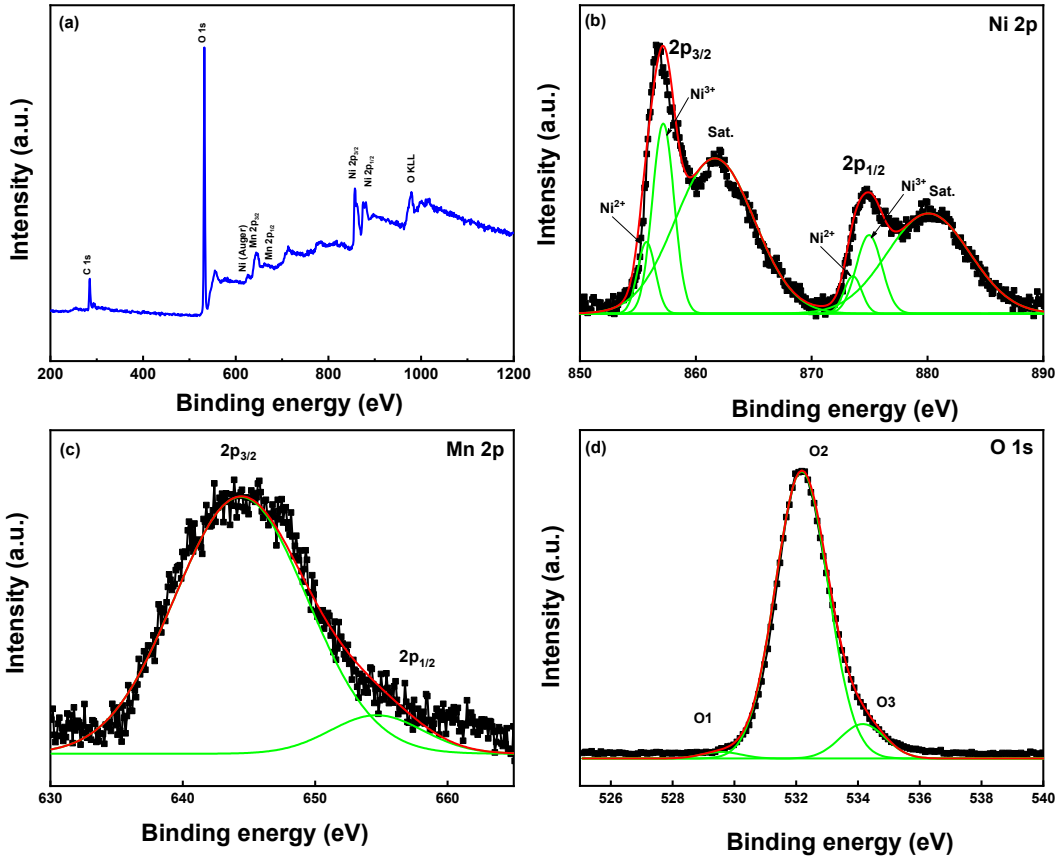

Figure S3. XPS a) survey and high-resolution spectra of b) Ni 2p, c) Mn 2p, and d) O 1s of the MNN heteronanostructure.

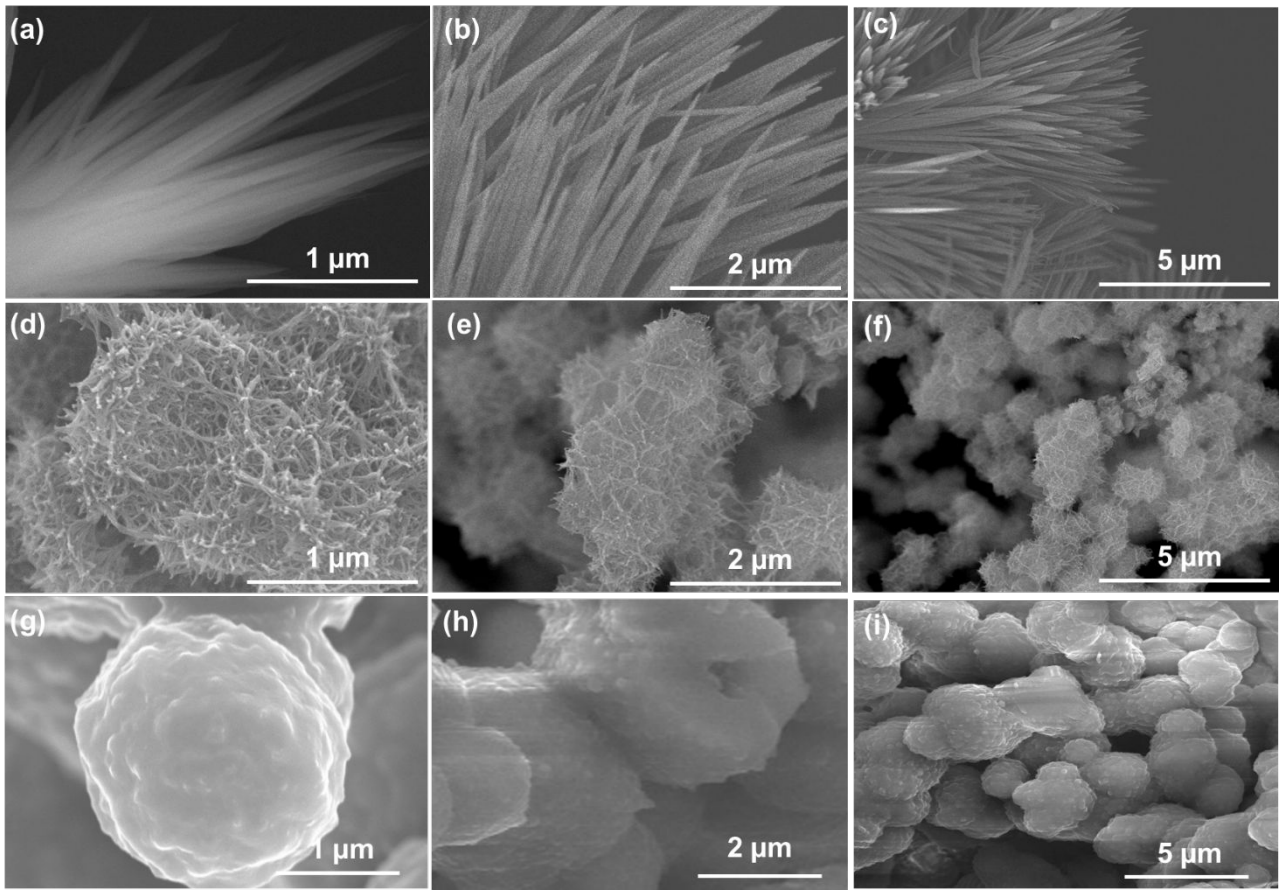

Figure S4. Low and high-magnification FE-SEM images of a-c) NC, d-f) NF and g-i) NM.

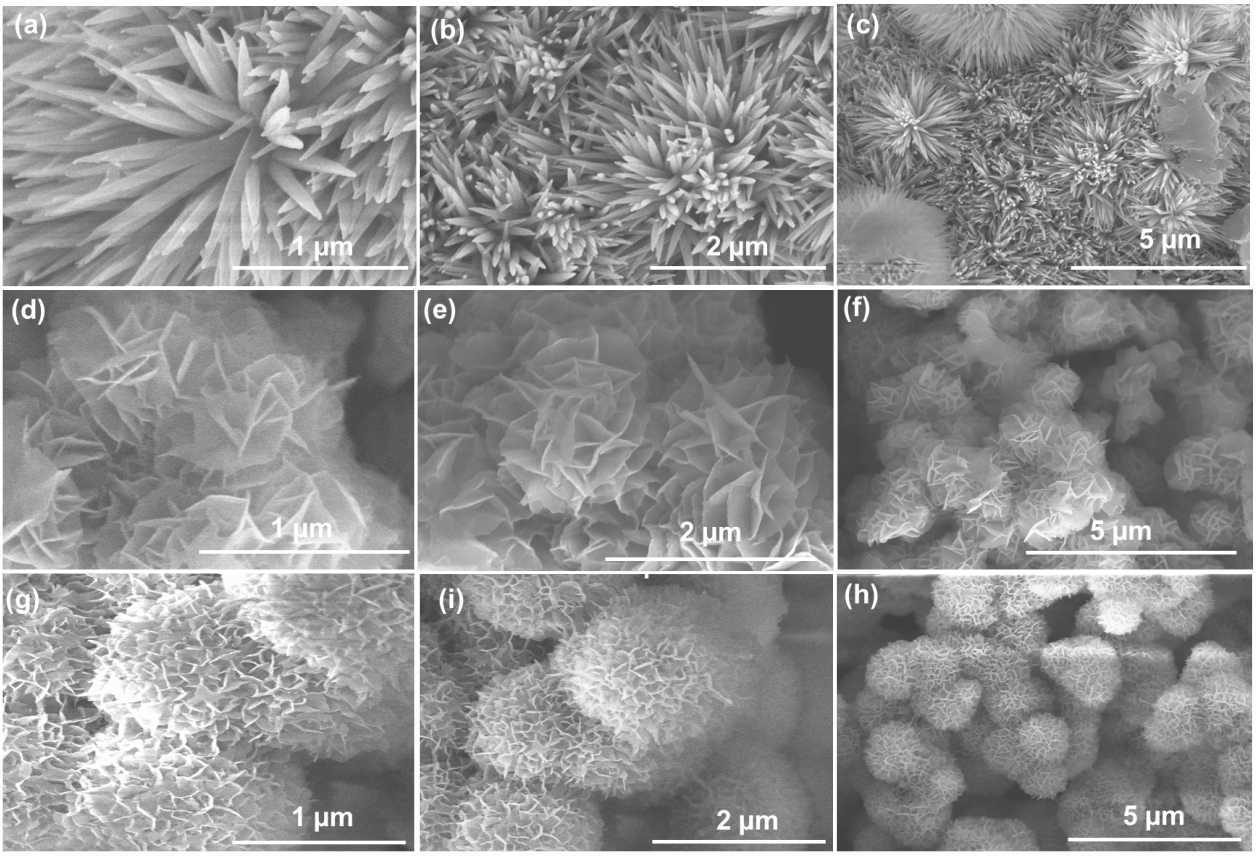

Figure S5. Low and high-magnification FE-SEM images of a-c) NCN, d-f) NFN and g-i) NMN.

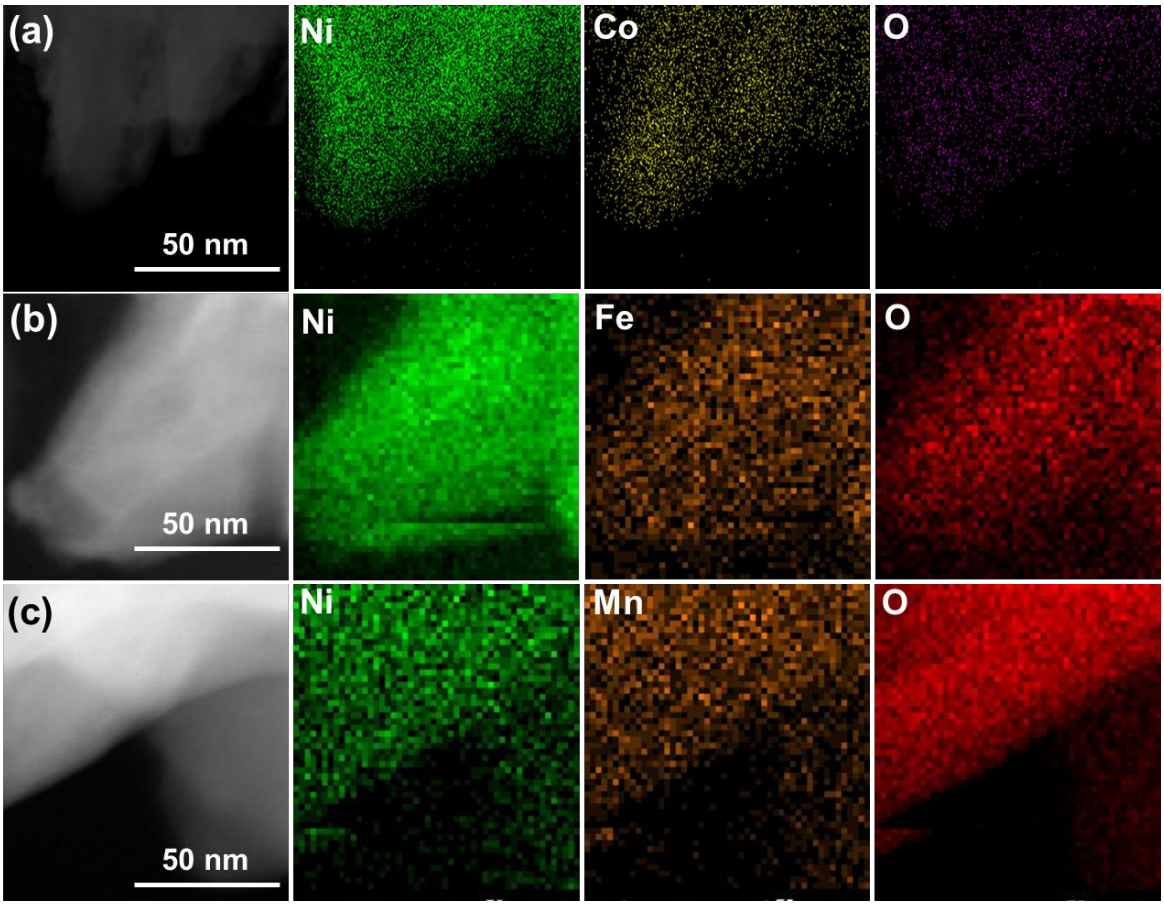

Figure S6. TEM elemental mapping of a) CNN, b) FNN and c) MNN heteronanostructures.

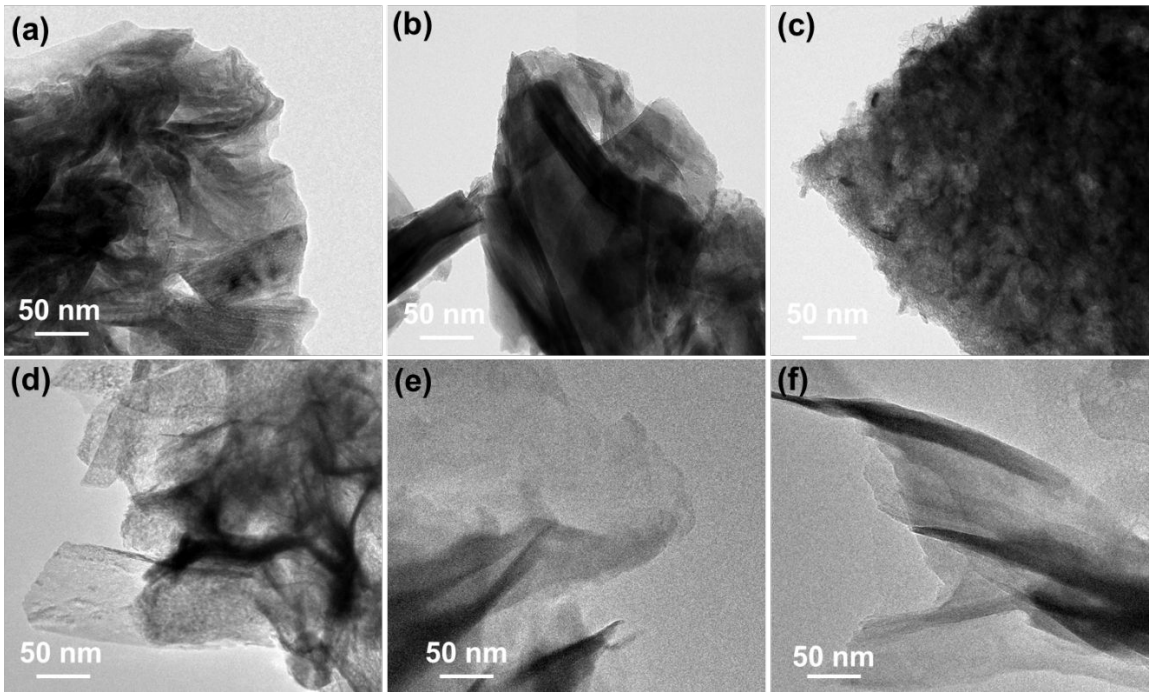

Figure S7. TEM images of a) NC, b) FC, c) MC, d) NCN, e) FCN and f) MCN.

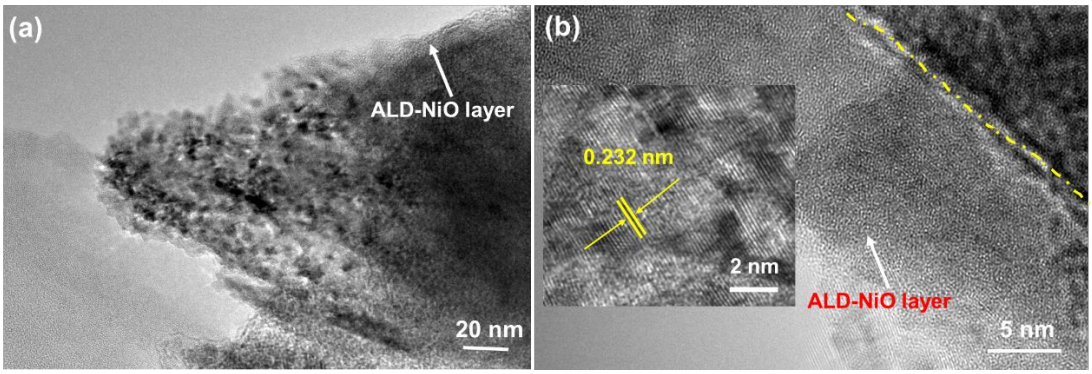

Figure S8. a-b) HR-TEM images of FNN heteronanostructure at different magnifications.

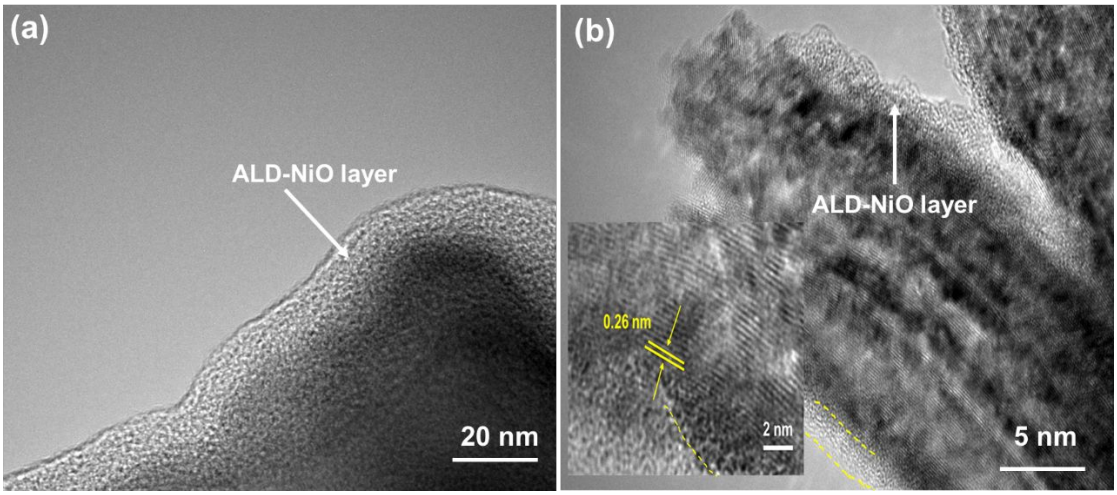

Figure S9. a-b) HR-TEM images of MNN heteronanostructure at different magnifications.

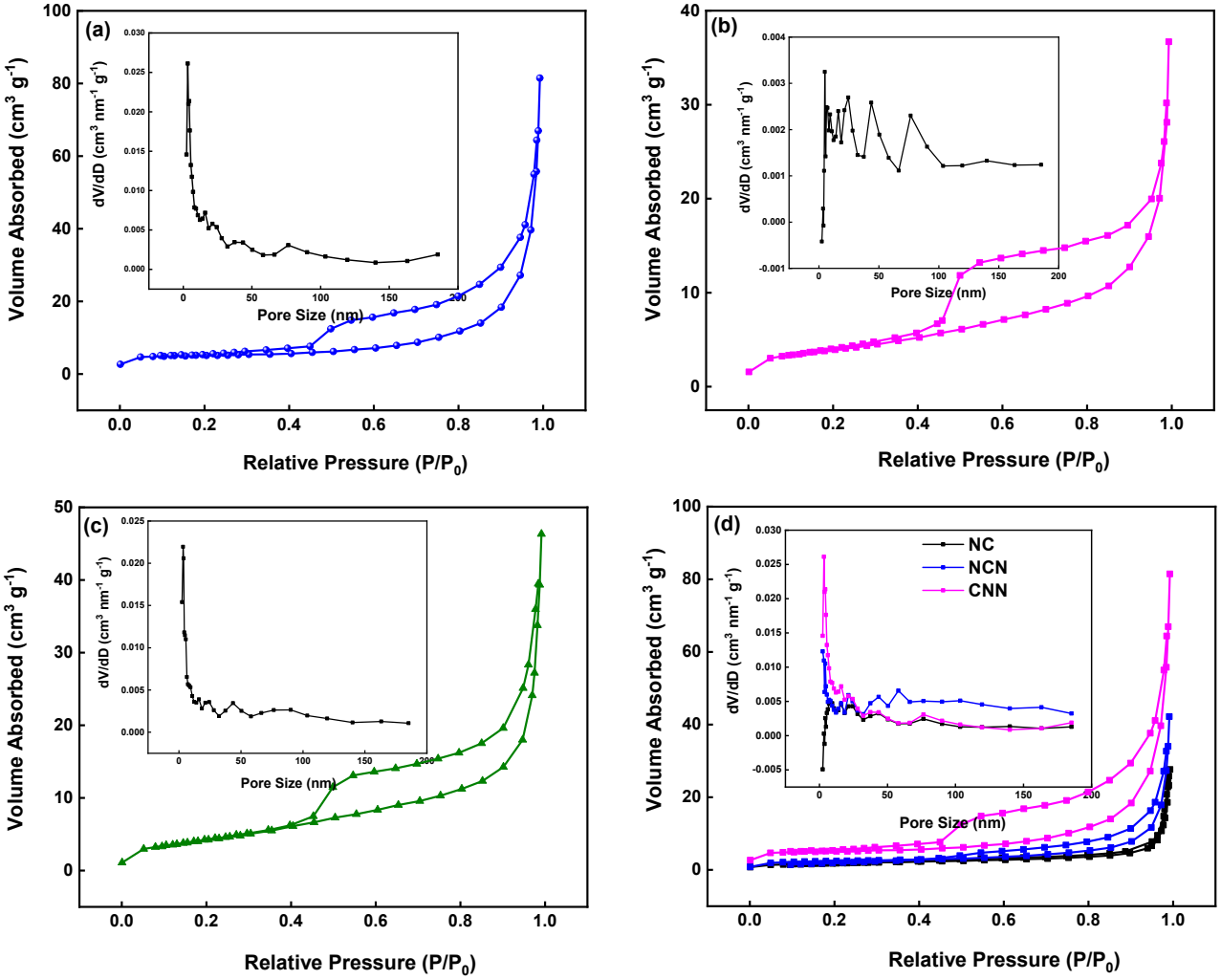

Figure S10. N_2 adsorption-desorption isotherms of a) CNN, b) FNN, c) MNN, and d) comparison of NC, NCN, CNN electrodes. Inset shows corresponding pore size distribution profiles.

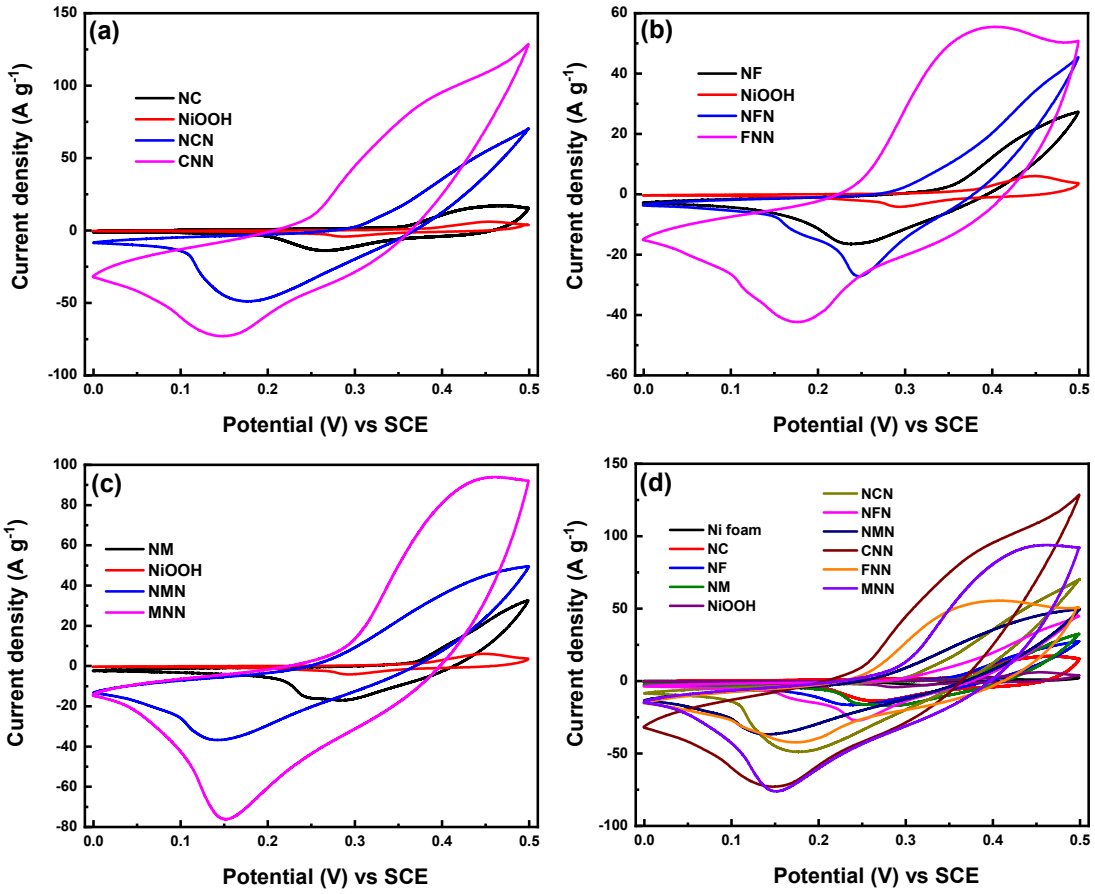

Figure S11. Comparison of a-c) CV profiles at 10 A g^{-1}. d) The comparative CV profiles of prepared electrodes at 10 mV s^{-1}.

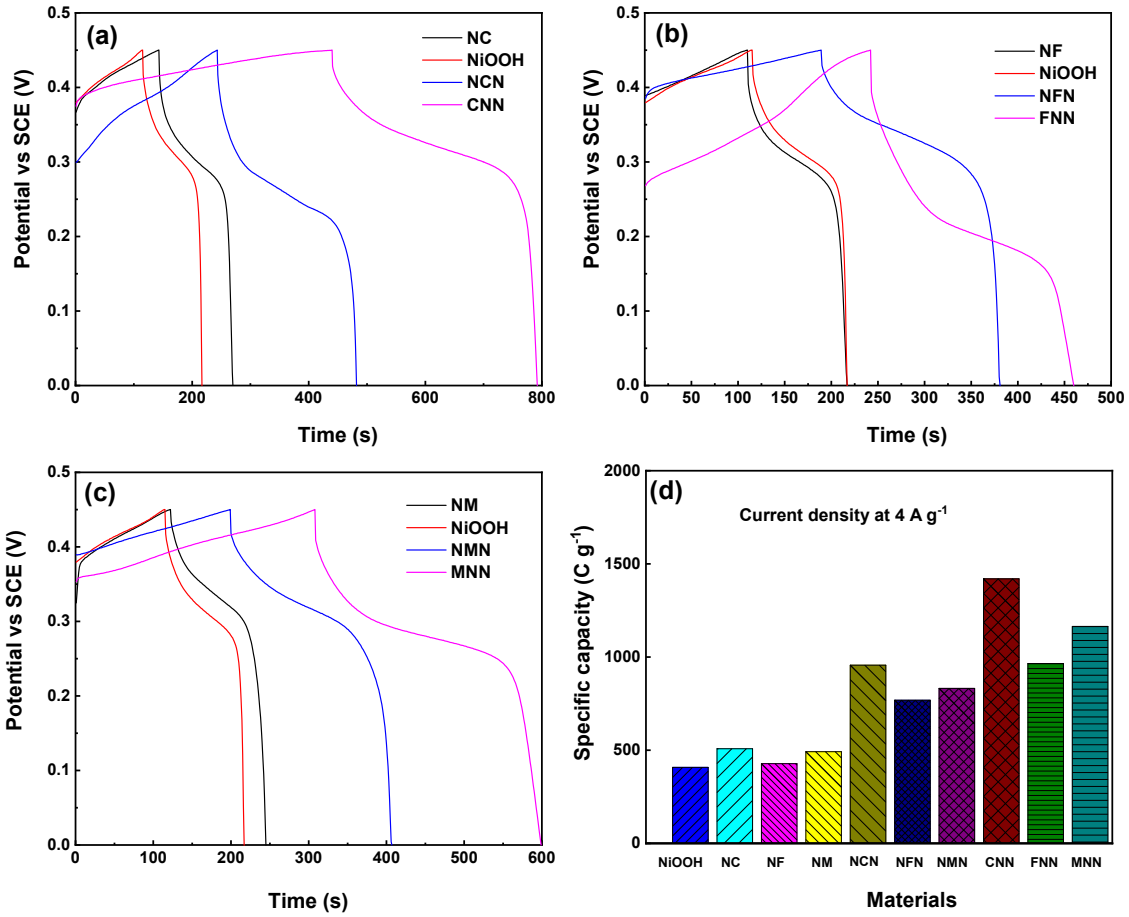

Figure S12. Comparison of a-c) GCD profiles at 4 A g^{-1} and d) specific capacity values of the prepared electrodes at 4 A g^{-1}.

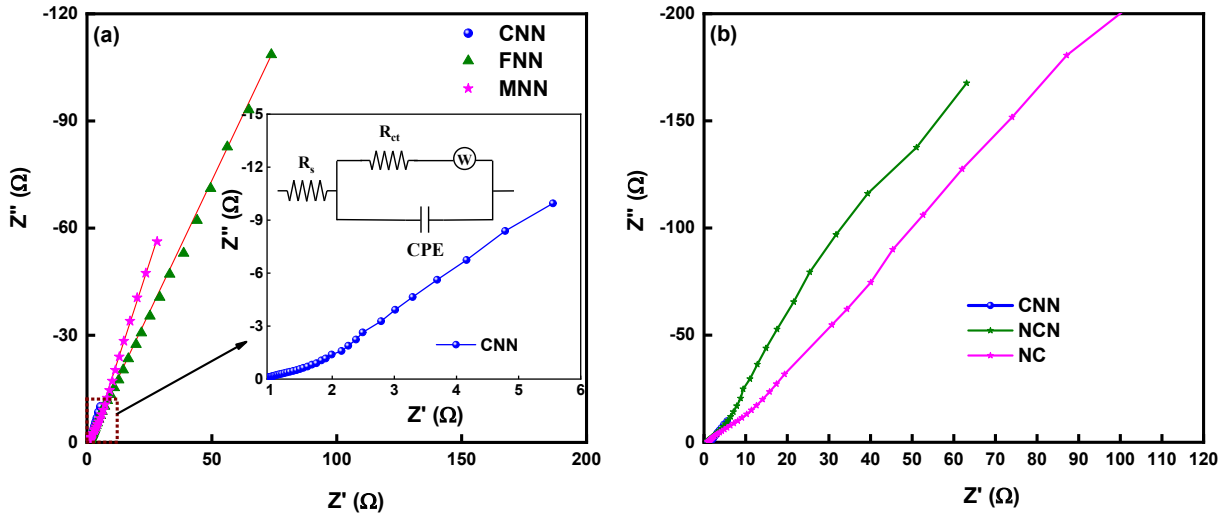

Figure S13. Nyquist plots of the a) NiX-LDH (X =Co, Fe and Mn)/NiOOH/ALD-NiO heteronanostructures. Inset shows expanded portion of CNN. b) Comparison of NC, NCN and CNN.

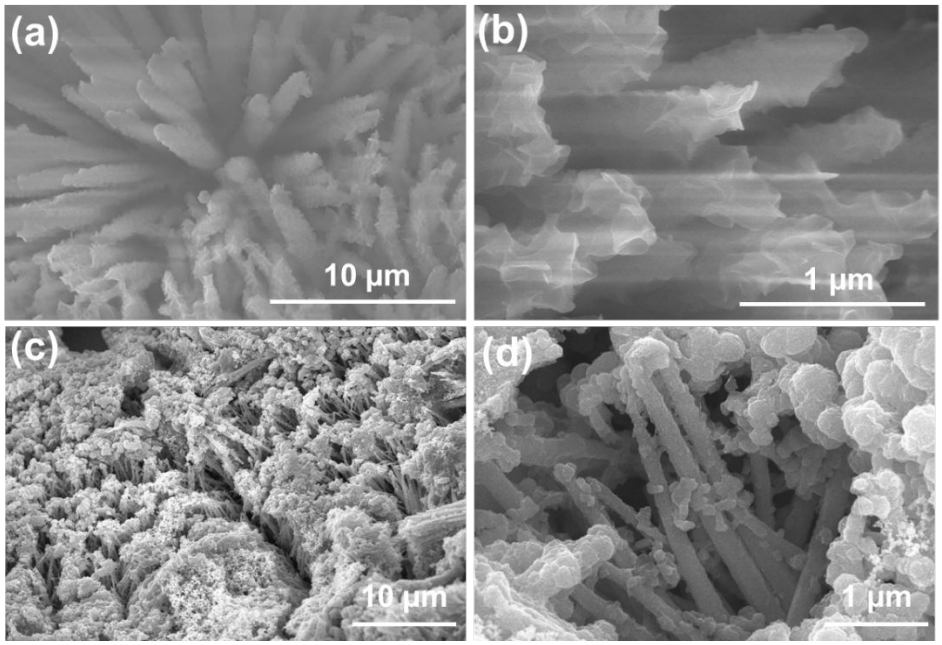

Figure S14. FE-SEM images of CNN heteronanostructure electrode a, b) before and c, d) after electrochemical cycling at two magnifications.

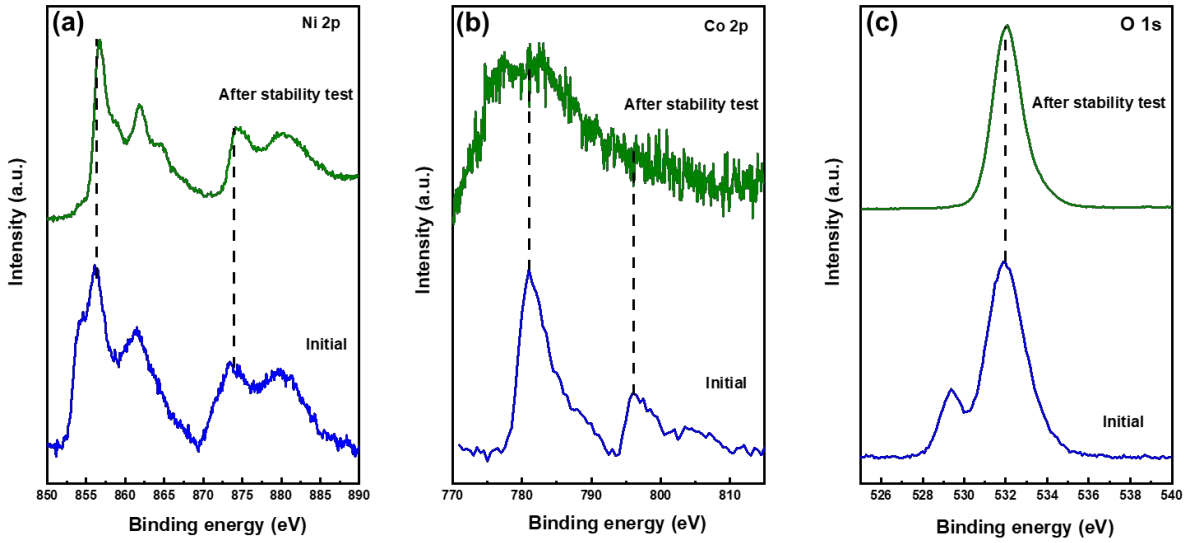

Figure S15. XPS spectra of a) Ni 2p, b) Co 2p and c) O 1s for CNN heteronanostructure before and after 20000 charge/discharge cycles.

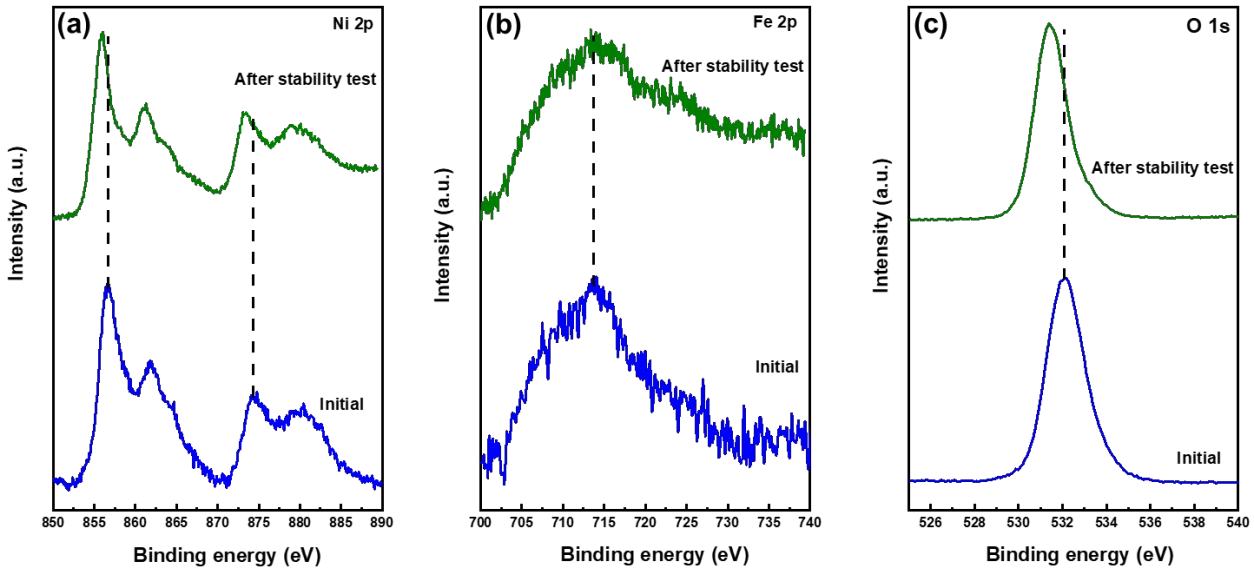

Figure S16. XPS spectra of a) Ni 2p, b) Fe 2p and c) O 1s for FNN heteronanostructure before and after 20000 charge/discharge cycles.

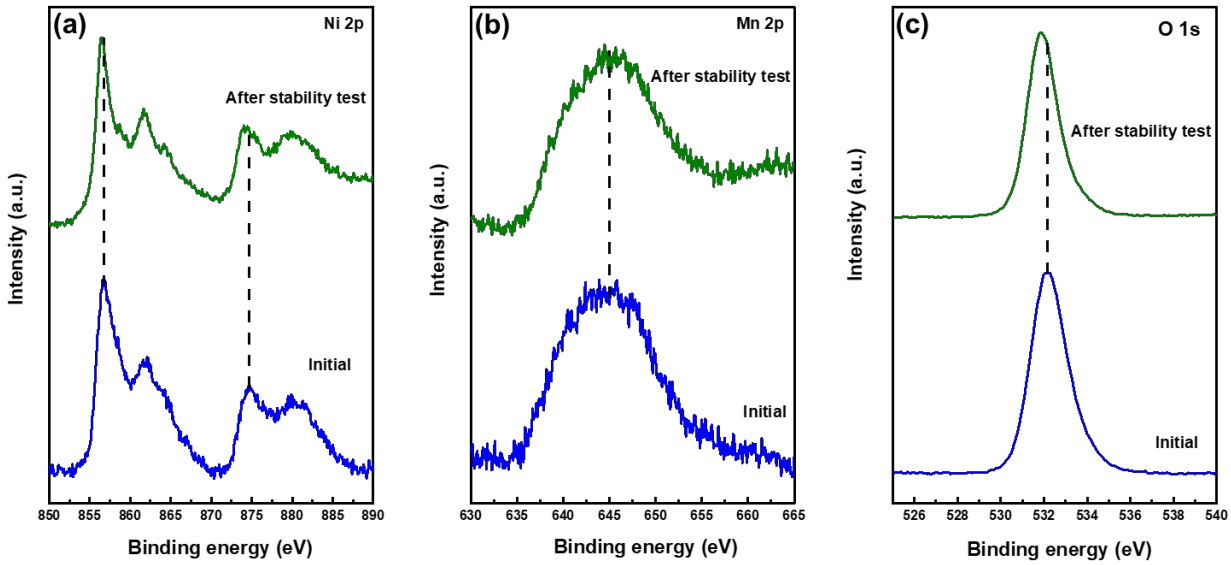

Figure S17. XPS spectra of a) Ni 2p, b) Mn 2p and c) O 1s for MNN heteronanostructure before and after 20000 charge/discharge cycles.

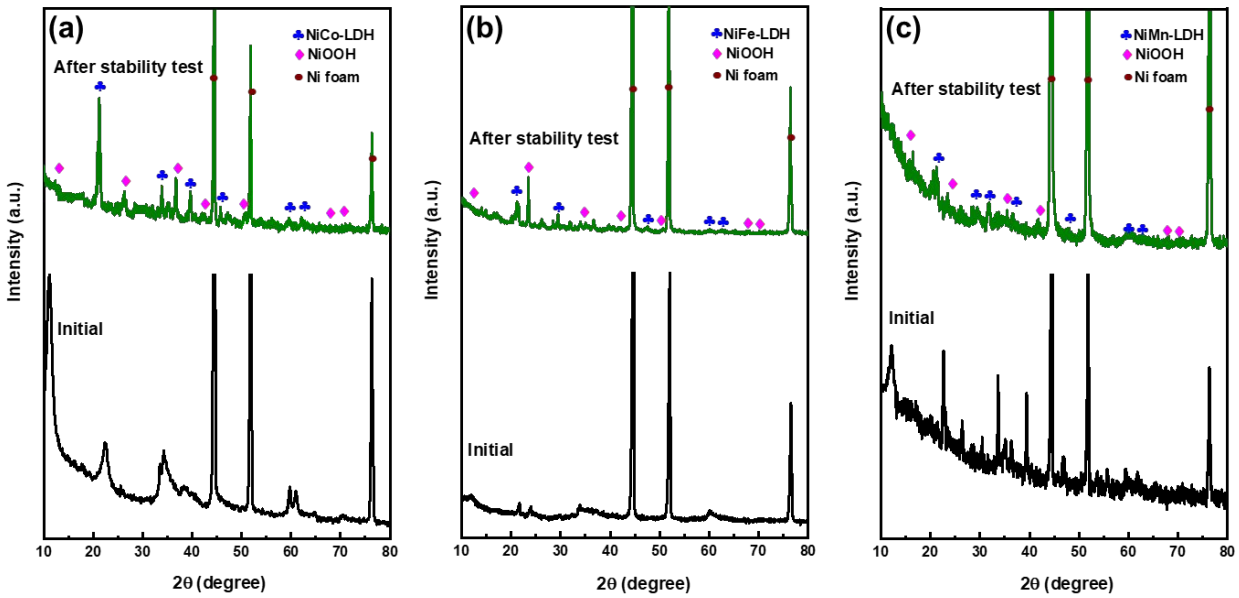

Figure S18. XRD patterns of a) CNN, b) FNN and c) MNN before and after 20000 charge/discharge cycles.

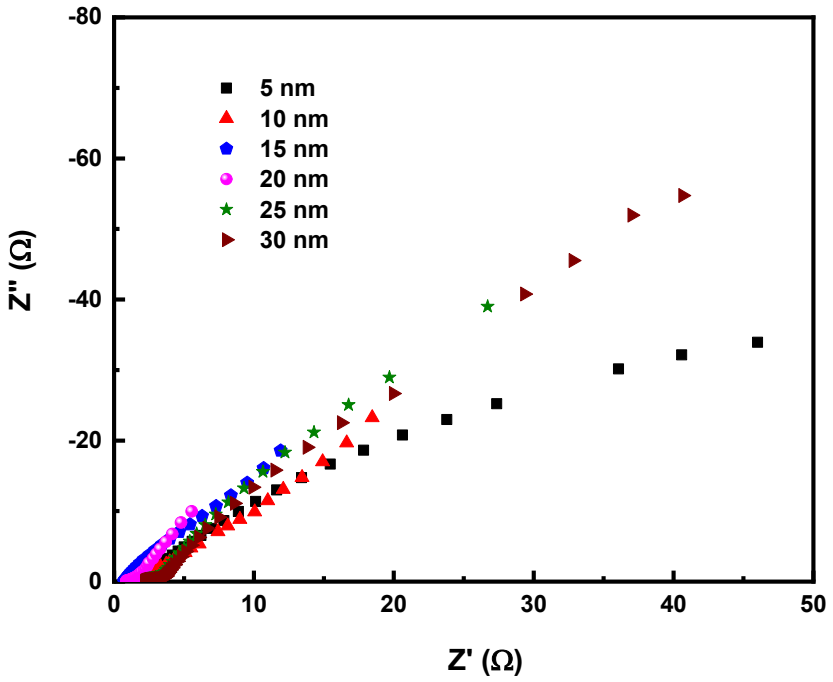

Figure S19. Nyquist plot of the CNN heteronanostructured electrode with different ALD-NiO coating thicknesses of 5, 10, 15, 20, 25 and 30 nm.

Table S1. Comparison of energy storage performances of LDH-based electrodes

Material	Fabrication method	Current collector	Electrolyte	C_s F g^{-1} (Current density A g^{-1})	Stability (Cycles)	Ref
Zn-Fe-Co ternary oxide nanowire	Hydrothermal and calcination	NF	6 M KOH	2587.4 (1 A g^{-1})	95.5% (3000)	1
Cu/CuO_xNW@$NiCo_2O_4$ NSs	Hydrothermal and calcination	NF	2 M KOH	578.0 (1 A g^{-1})	98.9% (6000)	2
Co_3O_4@$Ni(OH)_2$	Hydrothermal and calcination	NF	3 M KOH	1306.1 (1.2 A g^{-1})	90.0% (3000)	3
CCCH@NiCo-LDH@AuCuO/Cu fiber	Corrosion growth method.	Cu fiber	3 M KOH	1237.0	90.8% (30000)	4
CoMoS@$Co(OH)_2$	Hydrothermal and calcination	CC	3 M KOH	1711.0 (20 mA cm^{-2})	90.3% (5000)	5
SiCNWs@	electrodeposition	Carbon	2 M KOH	2580.0	-	6

$NiCo_2O_4/Ni(OH)_2$ HNAs	and calcination	Cloth		(4 A g^{-1})		
$NiO/NiCo_2O_4/Co_3O_4$	sol-gel process and calcination	NF	2 M KOH	1600.0 (2.5 A g^{-1})	94.9% (1000)	7
NiCo-OH/rGO	Hydrothermal	NF	6 M KOH	1316.0 (0.5 A g^{-1})	80.0% (17000)	8
$Ni(OH)_2$@Co/C	chemical bath deposition method	-	6 M KOH	929.0 (1 A g^{-1})	83.7% (10000)	9
$NiCo_2O_4$/NiO core-shell nanowire	Hydrothermal	Carbon cloth	2 M KOH	2439.0 (2 A g^{-1})	94.2% (20000)	10
NCNTs/ $Co_{0.5}Ni_{0.5}$-LDHs NSs	Electrodeposition	NF	2 M KOH	2170.0 (1 A g^{-1})	55.9% (5000)	11
$NiCo_2O_4$@NiO array	Hydrothermal and calcination	Metal substrate	1 M KOH	2220.0 (1 A g^{-1})	93.1% (3000)	12
Cactus-Like NiCoP/NiCo-OH	Hydrothermal	Carbon	3 M KOH	1100.0	97.0%	13

		cloth		(1 A g^{-1})	(1000)	
$CuCo_2O_4$@$Ni(OH)_2$ composites	hydrothermal treatment followed by electrochemical deposition	NF	6 M KOH	1902 .0 (2 A g^{-1})	87.6% (50000)	14
CoP/NiCoP	Seed growth method	NF	2 M KOH	1106.2 (1 A g^{-1})	100.0% 1000	15
CNTs@NCDHNs	Hydrothermal	NF	6 M KOH	1823.0 (1 A g^{-1})	-	16
(Ni,Co)Se_2/NiCo-LDH	Electrodeposition	Carbon cloth	3 M KOH	1224.0 (2 A g^{-1})	89.5% 3000	17
Co_3O_4@CoNi-LDH	Hydrothermal	NF	2 M KOH	2676.9 (0.5 A g^{-1})	67.7% 10000	18
NiCoLDH@NiOOH	Hydrothermal	carbon fiber cloth	6 M KOH	2622.0 (1 A g^{-1})	88.5% 10000	19

CNN heteronanostructure	**Hydrothermal/Chemical bath deposition/ALD**	**NF**	**2M KOH**	**3156.0 (1420.2 C g^{-1}) (4 A g^{-1})**	**93.0% (20000)**	**This work**
NF-Ni foam						

References

(1) Maitra, A.; Das, A. K.; Bera, R.; Karan, S. K.; Paria, S.; Si, S. K.; Khatua, B. B. An Approach To Fabricate PDMS Encapsulated All-Solid-State Advanced Asymmetric Supercapacitor Device with Vertically Aligned Hierarchical Zn-Fe-Co Ternary Oxide Nanowire and Nitrogen Doped Graphene Nanosheet for High Power Device Applications. *ACS Appl. Mater. Inter.* **2017,** *9* (7), 5947-5958.

(2) Kuang, M.; Zhang, Y. X.; Li, T. T.; Li, K. F.; Zhang, S. M.; Li, G.; Zhang, W. Tunable Synthesis of Hierarchical NiCo2O4 Nanosheets-Decorated Cu/CuOx Nanowires Architectures for Asymmetric Electrochemical Capacitors. *J. Power Sources* **2015,** *283*, 270-278.

(3) Bai, X.; Liu, Q.; Liu, J. Y.; Zhang, H. S.; Li, Z. S.; Jing, X. Y.; Liu, P. L.; Wang, J.; Li, R. M. Hierarchical Co3O4@Ni(OH)(2) Core-Shell Nanosheet Arrays for Isolated All- Solid State Supercapacitor Electrodes with Superior Electrochemical Performance. *Chem. Eng. J.* **2017,** *315*, 35-45.

(4) Guo, Y. Q.; Hong, X. F.; Wang, Y.; Li, Q.; Meng, J. S.; Dai, R. T.; Liu, X.; He, L.; Mai, L. Q. Multicomponent Hierarchical Cu-Doped NiCo-LDH/CuO Double Arrays for Ultralong-Life Hybrid Fiber Supercapacitor. *Adv. Funct. Mater.* **2019,** *29* (24), 1809004.

(5) Patil, S. J.; Lee, D. W. Scalable and Ascendant Synthesis of Carbon Cloth Coated Hierarchical Core-Shell CoMoS@Co(OH)(2) for Flexible and High-Performance Supercapacitors. *J. Mater. Chem. A* **2018,** *6* (20), 9592-9603.

(6) Zhao, J.; Li, Z. J.; Yuan, X. C.; Yang, Z.; Zhang, M.; Meng, A.; Li, Q. D. A High-Energy Density Asymmetric Supercapacitor Based on Fe2O3 Nanoneedle Arrays and NiCo2O4/Ni(OH)(2) Hybrid Nanosheet Arrays Grown on SiC Nanowire Networks as Free-Standing Advanced Electrodes. *Adv. Energy Mater.* **2018,** *8* (12), 1702787.

(7) Liu, M. C.; Kong, L. B.; Lu, C.; Li, X. M.; Luo, Y. C.; Kang, L. A Sol-Gel Process for Fabrication of NiO/NiCo2O4/Co3O4 Composite with Improved Electrochemical Behavior for Electrochemical Capacitors. *ACS Appl. Mater. Inter.* **2012,** *4* (9), 4631-4636.

(8) Ma, H. N.; He, J.; Xiong, D. B.; Wu, J. S.; Li, Q. Q.; Dravid, V.; Zhao, Y. F. Nickel Cobalt Hydroxide @Reduced Graphene Oxide Hybrid Nanolayers for High Performance Asymmetric Supercapacitors with Remarkable Cycling Stability. *ACS Appl. Mater. Inter.* **2016,** *8* (3), 1992-2000.

(9) Li, X. M.; Qiao, Y. Q.; Wang, C. H.; Shen, T. D.; Zhang, X. Y.; Wang, H. C.; Li, Y. S.; Gao, W. M. MOF-Derived CNC Nanocomposites Encapsulated by Ni(OH)(2) Ultrathin Nanosheets Shell for High Performance Supercapacitors. *J. Alloy. Compd.* **2019,** *770*, 803-812.

(10) Chodankar, N. R.; Selvaraj, S.; Ji, S. H.; Kwon, Y.; Kim, D. H. Interface-Engineered Nickel Cobaltite Nanowires through NiO Atomic Layer Deposition and Nitrogen Plasma for High-Energy, Long-Cycle-Life Foldable All-Solid-State Supercapacitors. *Small* **2019,** *15* (3), 1803716.

(11) Wu, J.; Liu, W. W.; Wu, Y. X.; Wei, T. C.; Geng, D. S.; Mei, J.; Liu, H.; Lau, W. M.; Liu, L. M. Three-Dimensional Hierarchical Interwoven Nitrogen-Doped Carbon Nanotubes/CoxNi1-x-Layered Double Hydroxides Ultrathin Nanosheets for High-Performance Supercapacitors. *Electrochim. Acta* **2016,** *203*, 21-29.

(12) Liu, X. J.; Liu, J. F.; Sun, X. M. NiCo2O4@NiO Hybrid Arrays with Improved Electrochemical Performance for Pseudocapacitors. *J. Mater. Chem. A* **2015,** *3* (26), 13900-13905.

(13) Li, X.; Wu, H. J.; Elshahawy, A. M.; Wang, L.; Pennycook, S. J.; Guan, C.; Wang, J. Cactus-Like NiCoP/NiCo-OH 3D Architecture with Tunable Composition for High-Performance Electrochemical Capacitors. *Adv. Funct. Mater.* **2018,** *28* (20), 1800036.

(14) Liu, W. M.; Chen, H.; Liao, H. Y.; Xiang, K. X.; Chen, W. H.; Li, X. Self-Supported Sisal-like CuCo2O4@Ni(OH)(2) Core-Shell Composites Grown on Ni Foam for High-Performance All-Solid State Supercapacitors. *Ind. Eng. Chem. Res.* **2019,** *58* (47), 21233-21241.

(15) Lin, Y.; Sun, K. A.; Liu, S. J.; Chen, X. M.; Cheng, Y. S.; Cheong, W. O.; Chen, Z.; Zheng, L. R.; Zhang, J.; Li, X. Y.; Pan, Y.; Chen, C. Construction of CoP/NiCoP Nanotadpoles Heterojunction Interface for Wide pH Hydrogen Evolution Electrocatalysis and Supercapacitor. *Adv. Energy Mater.* **2019,** *9* (36), 1901213.

(16) Wang, Y.; Wei, H. L.; Lv, H. F.; Chen, Z. X.; Zhang, J. J.; Yan, X. Y.; Lee, L.; Wang, Z. M. M.; Chueh, Y. L. Highly Stable Three-Dimensional Nickel-Cobalt Hydroxide Hierarchical Heterostructures Hybridized with Carbon Nanotubes for High-Performance Energy Storage Devices. *ACS Nano* **2019,** *13* (10), 11235-11248.

(17) Li, X.; Wu, H. J.; Guan, C.; Elshahawy, A. M.; Dong, Y. T.; Pennycook, S. J.; Wang, J. (Ni,Co)Se-2/NiCo-LDH Core/Shell Structural Electrode with the Cactus-Like (Ni,Co)Se-2 Core for Asymmetric Supercapacitors. *Small* **2019,** *15* (3), 1803895.

(18) Zhou, J.-J.; Li, Q.; Chen, C.; Li, Y.-L.; Tao, K.; Han, L. Co3O4@CoNi-LDH Core/Shell Nanosheet Arrays for High-Performance Battery-Type Supercapacitors. *Chem. Eng. J.* **2018,** *350*, 551-558.

(19) Liang, H. Y.; Lin, J. H.; Jia, H. N.; Chen, S. L.; Qi, J. L.; Cao, J.; Lin, T. S.; Fei, W. D.; Feng, J. C. Hierarchical NiCo-LDH@NiOOH Core-Shell Heterostructure on Carbon Fiber Cloth as Battery-Like Electrode for Supercapacitor. *J. Power Sources* **2018,** *378*, 248-254.